AGU PUBLICATIONS

Geophysical Research Letters

RESEARCH LETTER
10.1002/2016GL070974

**Key Points:**
- Addition of approximately 200 new stress orientations in Texas enables us to map the complex stress field throughout the state
- Recent earthquakes in four study areas occurred on critically stressed faults in which slip was apparently triggered by industrial activity

**Supporting Information:**
- Supporting Information S1
- Table S1–S2

**Correspondence to:**
J.-E. Lund Snee,
lundsnee@stanford.edu

**Citation:**
Lund Snee, J.-E., and M. D. Zoback (2016), State of stress in Texas: Implications for induced seismicity, *Geophys. Res. Lett.*, *43*, doi:10.1002/2016GL070974.

Received 24 AUG 2016
Accepted 28 SEP 2016
Accepted article online 2 OCT 2016



# State of stress in Texas: Implications for induced seismicity

**Jens-Erik Lund Snee[1] and Mark D. Zoback[1]**

[1]Department of Geophysics, Stanford University, Stanford, California, USA

**Abstract** Compilation of almost 200 new maximum horizontal stress ($S_{Hmax}$) orientations in Texas reveals a complex intraplate stress field. A large extensional stress province is associated with extensive growth faulting from northeastern Mexico to Louisiana. $S_{Hmax}$ is subparallel to the coastline, following the strikes of the growth faults. In contrast, we observe a strike-slip/normal faulting regime with $S_{Hmax}$ approximately E-W in much of west Texas and the Texas Panhandle, similar to the stress fields observed in northeast New Mexico and north-central Oklahoma. Within the Fort Worth Basin in northeast Texas, $S_{Hmax}$ is NNE-SSW. The faulting regime transitions from strike-slip/normal faulting in the northern part of the basin to normal faulting with subequal horizontal principal stress magnitudes further south. Recent sites of apparently injection-related seismicity near Snyder/Cogdell (west Texas), Karnes City/Fashing (south Texas), the Dallas-Fort Worth metroplex, and Timpson (east Texas) involves fault slip compatible with local stress fields.

## 1. Introduction

In this paper we discuss regional variations of the state of stress in Texas and active faulting associated with recent seismicity in the state. Approximately 200 new $S_{Hmax}$ orientations reveal a complex stress field that has implications for understanding seismic hazard and the possibility of earthquake triggering throughout the state. Decades ago, compilations of crustal stress data revealed large provinces with remarkably consistent stress orientations and faulting regimes (relative stress magnitudes) [e.g., *Zoback and Zoback*, 1980, 1989; *Zoback*, 1992]. Despite continuous progress mapping stress orientations and relative magnitudes around the world [e.g., *Heidbach et al*., 2010], stress information in many areas remains sparse. Prior to this study, fewer than 30 reliable $S_{Hmax}$ orientations were available in the World Stress Map database in Texas. In the sections below, we first briefly review the methods we employ for obtaining and analyzing the stress data and then present observations arising from the new data. We then utilize the new stress data to better understand faulting associated with apparently triggered earthquakes at four sites.

## 2. Stress Map of Texas

We employ established techniques for determining in situ $S_{Hmax}$ orientations from drilling-induced tensile fractures and borehole breakouts observed in wellbore image logs, maximum horizontal shear wave velocity from crossed-dipole sonic logs, and hydraulic fractures from microseismic data (see review in *Zoback* [2010]). Most of our $S_{Hmax}$ orientations (Table S1) were measured in supracrustal rocks, but nearly all were collected at more than 1 km depth. We interpret faulting regime (e.g., normal, strike-slip, or reverse) from in situ measurements, geologic data, and moment tensors from Saint Louis University [*Herrmann et al.,* 2011] and local studies [*Doser et al.,* 1991; *Hornbach et al.,* 2015] (Table S2). We categorize faulting regime using the $A_\varphi$ system of *Simpson* [1997], in which increasing $A_\varphi$ represents more compressive conditions, with 0 denoting radial extension (normal faulting with $S_V \gg S_{Hmax} = S_{hmin}$) and 3 denoting radial compression (reverse faulting with $S_{Hmax} = S_{hmin} \gg S_V$).

Figure 1 shows $S_{Hmax}$ orientations and faulting regime compiled across Texas and surrounding areas. $S_{Hmax}$ orientations include previously obtained measurements in Oklahoma compiled by *Alt and Zoback* [2016] and three unpublished measurements from the World Stress Map compilation (O. Heidbach, personal communication, 2016). We exclude single moment tensor solutions used to obtain approximate principal stress orientations. Relative stress magnitudes ($A_\varphi$ values) in central Oklahoma are from moment tensor inversions by *Walsh and Zoback* [2016]. In addition, we conducted a formal inversion of Saint Louis University (SLU) moment tensors in the Raton Basin using the iterative joint inversion method of *Vavryčuk* [2014], and we include other relative stress magnitudes from outside of Texas compiled by *Hurd and Zoback* [2012] in order

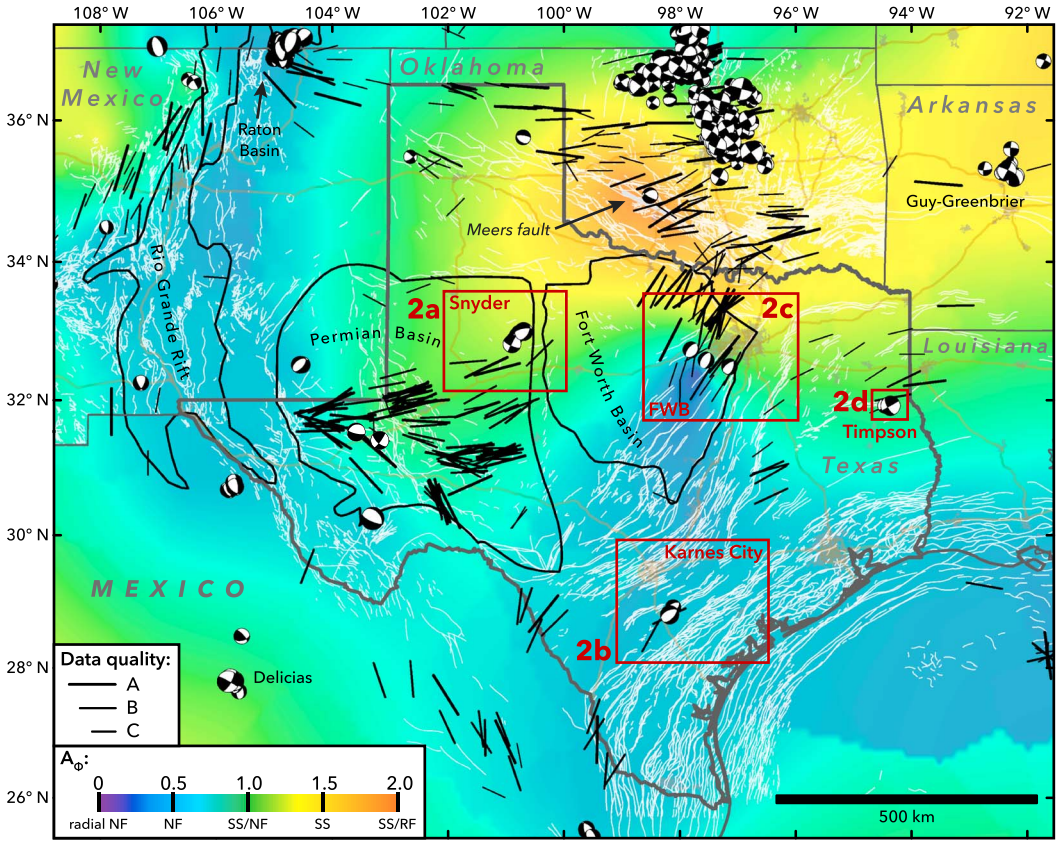


**Figure 1.** Stress Map of Texas showing maximum horizontal stress ($S_{Hmax}$) orientations and faulting regime categorized using the $A_\varphi$ system of *Simpson* [1997] (see text for details). Basin boundaries are from the U.S. Energy Information Administration. The Rio Grande Rift boundary was compiled from *Seager and Morgan* [1979] and *Perry et al.* [1987]. RF, reverse faulting; SS, strike-slip faulting; and NF, normal faulting.

to limit edge effects. Fault traces are compiled from *Ewing et al.* [1990], *Ewing and Lopez* [1991], *Green and Jones* [1997], and *Darold and Holland* [2015].

From west to east in Figure 1, we see that $S_{Hmax}$ is ~ N-S in the vicinity of the extensional, ~N-S trending Rio Grande Rift in central New Mexico. $S_{Hmax}$ transitions rapidly eastward to ~ E-W in northeast New Mexico, the Texas Panhandle, and the Permian Basin of west Texas. Continuing eastward, $S_{Hmax}$ rotates from E-W in the western Permian Basin to NNE-SSW (~N020°E) in the Fort Worth Basin of northeast Texas. $S_{Hmax}$ then rotates sharply to nearly E-W in south-central Oklahoma, where there is excellent agreement between $S_{Hmax}$ azimuths calculated from inversions of dozens of moment tensors (typically 5–6 km depth) and those measured in boreholes drilled in sedimentary rocks to depths of ~2.5 km [*Walsh and Zoback*, 2016]. The E-W $S_{Hmax}$ in Oklahoma transitions further east to the generally NE-SW to NNE-SSW $S_{Hmax}$ observed across most of the central and eastern United States, which experience strike-slip and reverse faulting [*Zoback and Zoback*, 1980; *Hurd and Zoback*, 2012]. In east Texas and western Louisiana, $S_{Hmax}$ is distinctly more easterly than in the Fort Worth Basin.

In general, along the Gulf Coast of southern Texas and Louisiana and eastern Mexico, $S_{Hmax}$ is subparallel to the coastline and extensive growth faulting accommodates extension of the post-Jurassic sedimentary succession into the Gulf of Mexico [*Zoback and Zoback,* 1980]. Approximately Gulf Coast-parallel $S_{Hmax}$ continues northwestward into the southeastern part of the Permian Basin in west Texas. Intriguingly, in that area, $S_{Hmax}$ changes rapidly from NE-SW in the south to NW-SE on the west (counter-clockwise rotation westward) and E-W further north in the Permian Basin (clockwise rotation northward).

Relative stress magnitudes also vary across Texas (Figure 1). Active ~ E-W extension is associated with the Rio Grande Rift in New Mexico [*Ricketts et al*., 2014] and northeastern Mexico. In west Texas the faulting regime is

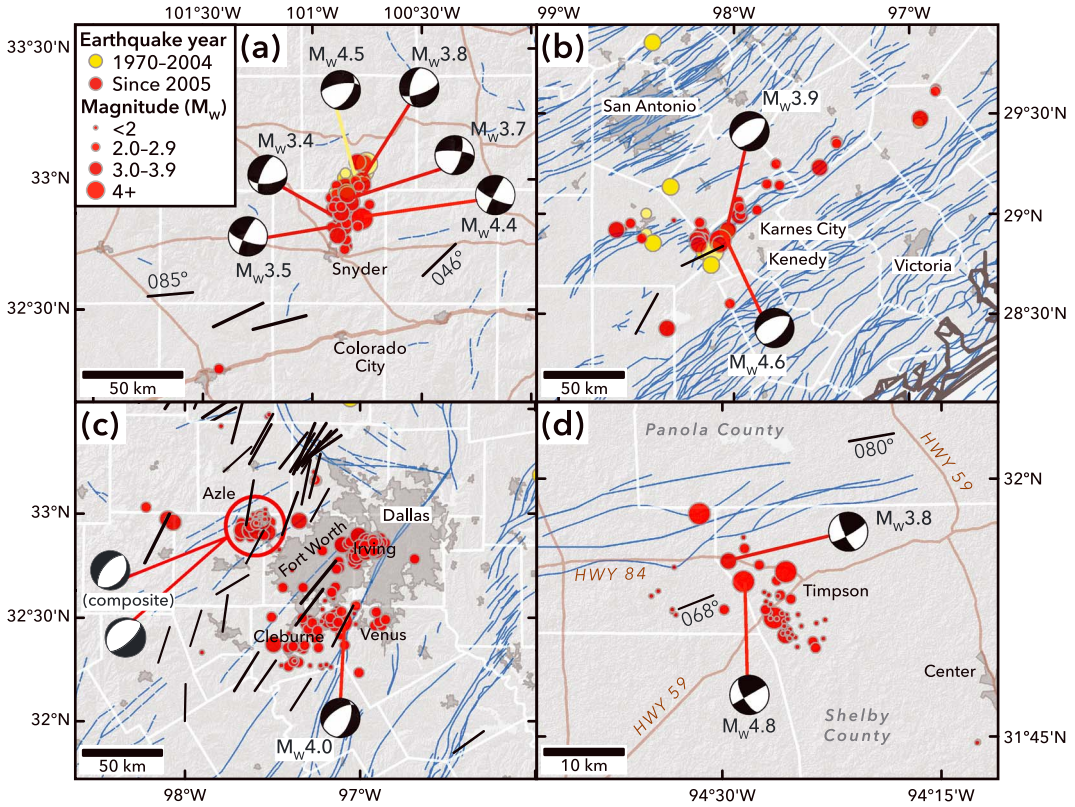


**Figure 2.** Maps of earthquakes in Texas compiled from *Frohlich et al.* [2011], *Frohlich and Brunt* [2013], *Gan and Frohlich* [2013], *Justinic et al.* [2013], *Frohlich et al.* [2014], *Hornbach et al.* [2015], *Walter et al.* [2016], and the U.S. Geological Survey National Earthquake Information Center. (a) Snyder/Cogdell; (b) Karnes City/Fashing; (c) Dallas-Fort Worth metroplex; (d) Timpson. Composite moment tensors in (Figure 2c) are from *Hornbach et al.* [2015]. Locations of these four areas are shown in Figure 1.

more compressional. East-west compression and both normal and strike-slip focal mechanisms are seen in the Texas Panhandle, north Texas near Snyder, and the western Permian Basin [*Doser et al.*, 1991; *Herrmann et al.*, 2011]. Two recent strike-slip focal mechanisms were recorded in east Texas near Timpson, together suggesting a strike-slip/normal faulting regime. *Fan et al.* [2016], and references therein, independently determined a strike-slip/normal faulting regime in a nearby borehole. Further west, in situ measurements and inversion of microseismic data show that the stress regime transitions northward in the Fort Worth Basin from normal faulting with nearly isotropic horizontal stress magnitudes ($A_\varphi = 0.18$) [*Vermylen and Zoback*, 2011] to strike-slip/normal faulting ($A_\varphi = 0.81$) (W. Kuang, personal communication, 2016) to strike slip ($A_\varphi = 1.50$) [*Sone and Zoback,* 2014]. The faulting regime becomes increasingly compressive northward into southwest Oklahoma, as paleoseismic studies [*Madole,* 1988; *Crone and Luza,* 1990] have shown that the Meers fault (Figure 1) produces oblique reverse/strike-slip earthquakes, although a single oblique strike-slip/normal faulting earthquake ($M_w$3.9) has been recorded nearby.

## 3. Implications for Faulting Associated With Seismicity

As in other parts of the central and eastern United States, the rate of seismicity in Texas has markedly increased since 2009 [*Frohlich et al.,* 2016]. Constraining the stress state enables retrospective analysis of earthquake triggering mechanisms, as well as quantitative assessment of the likelihood of slip on known faults due to fluid pressure perturbations. We apply our new stress data to conduct basic Mohr-Coulomb failure analyses for four areas that have experienced recent seismicity in Texas, and we calculate the pore pressure change, $\Delta P_P$, that would have been required to trigger slip, assuming that perfectly oriented faults are in frictional equilibrium. Whether or not a given earthquake was triggered by injection-related pressure changes, the likely fault plane in any given focal plane mechanism is that most well oriented for failure in

**Table 1.** Results of Geomechanical Analysis of the Snyder and Timpson, Texas, Earthquakes

| Earthquake | Nodal Plane Orientation | $S_{Hmax}$ Orientation | $\Delta P_P$ to Failure (MPa/km) | $\Delta P_P$ to failure at 5 km depth (MPa) |
|---|---|---|---|---|
| | | *Snyder, Texas* | | |
| 16 June 1978 | 260°/60° | N046°E | 1.48 | 7.40 |
| $M_w$4.5 | | N066°E | 0.72 | 3.59 |
| | | N085°E | 0.79 | 3.93 |
| | 031°/41° | N046°E | 2.88 | 14.39 |
| | | N066°E | 4.28 | 21.39 |
| | | N085°E | 6.88 | 34.41 |
| 11 September 2011 $M_w$4.4 | 115°/70° | N046°E | 8.16 | 40.81 |
| | | N066°E | 2.85 | 14.24 |
| | | N085°E | 0.44 | 2.19 |
| | 207°/85° | N046°E | 0.62 | 3.09 |
| | | N066°E | 0.57 | 2.85 |
| | | N085°E | 4.47 | 22.33 |
| Earthquake/Fault | Nodal Plane Orientation | $S_{Hmax}$ Orientation | $\Delta P_P$ to Failure (MPa/km) | $\Delta P_P$ to Failure at 2.5 km Depth (MPa) |
| | | *Timpson, Texas* | | |
| 17 June 2012 $M_w$4.8 | 060°/90° | N068°E | 2.70 | 6.76 |
| | | N074°E | 1.54 | 3.85 |
| | | N080°E | 0.72 | 1.81 |
| | 150°/60° | N068°E | 12.23 | 30.59 |
| | | N074°E | 10.60 | 26.50 |
| | | N080°E | 8.93 | 22.34 |
| 10 June 2012 $M_w$3.8 | 060°/76° | N068°E | 1.07 | 2.68 |
| | | N074°E | 0.65 | 1.62 |
| | | N080°E | 0.29 | 0.73 |
| | 155°/70° | N068°E | 13.41 | 33.52 |
| | | N074°E | 11.72 | 29.30 |
| | | N080°E | 9.93 | 24.82 |
| Mapped fault | 138°/63° | N068°E | 8.76 | 21.90 |
| | | N074°E | 7.08 | 17.70 |
| | | N080°E | 5.50 | 13.74 |

the current stress field. Equivalently, this plane would require the smallest $\Delta P_P$ if the event was triggered by fluid injection.

For each of the recent earthquake sequences considered here (Figure 2), at least one of the fault planes and senses of slip shown in the focal mechanisms is consistent with the local stress field and would have required relatively small changes of pore pressure to be triggered. The 1978–2016 earthquakes near Snyder, Texas, produced moment tensors with nodal planes striking mostly N and E for the strike-slip events and NE for the oblique normal faulting events, as well as a NNE-trending group of event locations (Figure 2a). These fault orientations are consistent with nearby in situ measurements showing NE-SW $S_{Hmax}$ orientations. Most of the events occurring during and after 2006 in this area may have been triggered by injection of supercritical $CO_2$ in the Cogdell oilfield [*Gan and Frohlich*, 2013], and the earlier events may have been triggered by oilfield water flooding operations [*Davis and Pennington*, 1989]. We estimate the pressure perturbation ($\Delta P_P$) needed to achieve failure for both nodal planes of the two largest earthquakes in this area (16 June 1978 $M_w$4.5 and 11 September 2011 $M_w$4.4, shown in Figure 2a), assuming hydrostatic pore pressure ($P_P$) and critically stressed conditions for $A_\varphi = 1.2$ (Figure 1). $S_{Hmax}$ varies from N046°E to N085°E, which is a large enough range to change which of the two nodal planes is expected to represent the slipping fault in the case of the 2011 $M_w$4.4 event. Across this range of $S_{Hmax}$ orientations at a reasonable hypocenter depth of 5 km, $\Delta P_P$ ranges from 3.6 to 7.4 MPa for the NW dipping nodal plane and from 14.4 to 34.4 MPa for the SE dipping nodal plane associated with the 1978 $M_w$4.5 earthquake (Table 1). At the same depth and range of $S_{Hmax}$ orientations, we estimate $\Delta P_P$ of 2.8–22.3 MPa and 2.2–40.8 MPa, respectively, for the NW and SW dipping nodal planes produced by the 2011 $M_w$4.4 earthquake. These results demonstrate the sensitivity of earthquake triggering studies to variations in the local stress field. In Figure 3a, we show the estimated $\Delta P_P$ needed to produce slip on

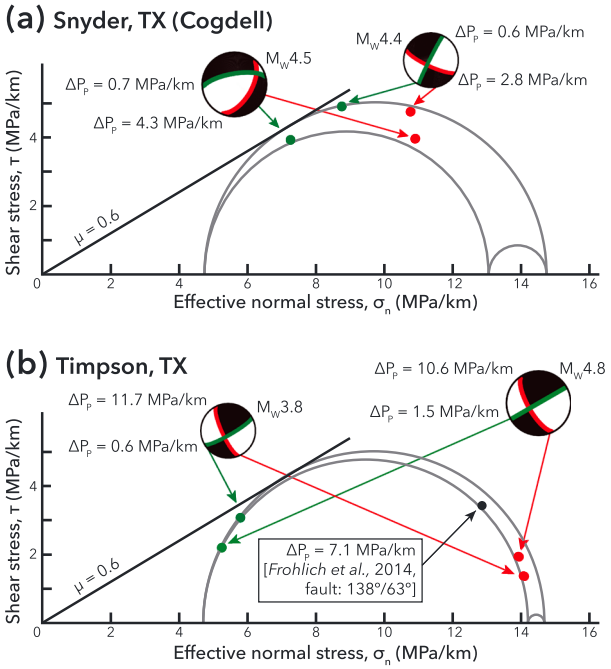


**Figure 3.** (a) Mohr circle showing stress conditions near Snyder, Texas. Saint Louis University (SLU) focal mechanisms are shown for the two largest events [*Herrmann et al.*, 2011], and resolved shear and normal stresses are shown for each nodal plane. (b) Mohr circle showing stress gradients in the Timpson area based on stress and pore pressure estimates from *Fan et al.* [2016].

each nodal plane for these two earthquakes assuming an average $S_{Hmax}$ orientation of N066°E. In this figure, horizontal distance between a plane and the Coulomb failure line represents the $\Delta P_P$ needed to trigger fault slip. For this intermediate $S_{Hmax}$ orientation at 5 km depth, we estimate that fairly modest $P_P$ increases of 3.6 MPa and 2.8 MPa, respectively, were needed to trigger the 1978 $M_w$4.5 and 2011 $M_w$4.4 earthquakes.

Two earthquakes in 2008 and 2011 near Karnes City, Texas, which may have been triggered by production from wells in the Fashing gas field [*Frohlich and Brunt*, 2013], generated moment tensors that indicate slip on NE striking planes (Figure 2b). Normal slip on NE striking planes is in agreement with the NE-SW $S_{Hmax}$ orientations and the trend of normal faults along this part of the Gulf Coast (Figure 1). Possibly triggered normal faulting earthquakes have also recently occurred in the Dallas-Fort Worth area, including a 2013-2014 sequence near Azle and a 2015 $M_w$4.0 event near Venus [*Hornbach et al.*, 2015, 2016]. These events involve normal faulting on NE striking planes that is consistent with both the stress field and the mapped faults in the region (Figure 2c). However, as noted above, the faulting regime in the Fort Worth Basin appears to change from mostly strike-slip north of Fort Worth, to normal/strike slip near Dallas and Fort Worth, to normal faulting further south (Figure 1). This transition presents important implications for seismic hazard analysis in the Dallas-Fort Worth metroplex because different sets of faults would be expected to be active in different parts of the basin (Figure 2c).

Finally, seismicity in 2012 near Timpson, Texas, produced two strike-slip moment tensors with NW and NE striking nodal planes, as well as a sequence of NW and NE trending aftershocks, suggesting slip along a previously mapped NW striking fault [*Frohlich et al.*, 2014, and references therein] and/or multiple NE striking faults. The original SLU focal mechanisms showed orthogonal *P* axes, suggesting that two earthquakes occurring days apart (10 June 2012 and 17 June 2012) were produced either from strike-slip on perpendicular faults or from opposite shear senses on parallel faults. This unusual scenario implied either a dramatically varying local stress field or slip on an unfavorably oriented fault induced by severely elevated pore pressure. Using a geomechanical model that accounted for poroelastic stress changes, *Fan et al.* [2016] found that slip on the NW striking mapped fault could have been triggered by a large pore pressure perturbation (12.9 MPa near 1800 m depth) resulting from nearby injection of saline wastewater. Our new stress data show that $S_{Hmax}$ orientations are generally consistent across that area, ranging from N068°E to N080°E (Figure 2d). In addition, both moment tensors were subsequently recalculated on 23 June 2016 using a more refined local velocity model [see *Herrmann,* 2016], resulting in two strike-slip focal mechanisms with similar nodal plane and *P* axis orientations to one another (Figure 2d). Geomechanical analysis of the four nodal planes and the NW striking mapped fault (Figure 3b) shows that the NE striking nodal planes are near ideal orientations for slip in the local stress field. At the ~2.5 km top-fault depth shown by *Frohlich et al.* [2014], only 1.8–6.8 MPa $\Delta P_P$ in the case of the 17 June 2012 $M_w$4.8 earthquake and 0.7–2.7 MPa $\Delta P_P$ for the 10 June 2012 $M_w$3.8 earthquake were needed to trigger slip (Table 1). In contrast, the NW striking fault and nodal planes have highly unfavorable orientations, requiring a minimum 13.7 MPa pressure increase. *Fan et al.* [2016] demonstrate that poroelastic stress changes could allow $P_P$ to build to the point that a severely misoriented fault could slip, but

a requirement of their model is that no well-oriented faults are present. As shown above, only modest $\Delta P_P$ changes would be required to trigger slip on the well-oriented NE striking nodal planes. We consider it unlikely that a pore pressure perturbation large enough to trigger slip on the NW striking planes could occur without first hydraulically fracturing the formations near the well or triggering slip on the more well-oriented NE-ENE striking faults mapped nearby (Figure 2d). Moreover, we do not consider poroelasticity because modeling poroelastic stress changes is not straightforward if the $P_P$ changes occur preferentially in fracture networks rather than being widely distributed in the formation.

## 4. Conclusions

The new stress measurements presented here reveal a complex but spatially coherent stress field in Texas, which allows us to better understand the triggering mechanisms of past earthquakes and to characterize the seismic hazard across the area. Although Texas is relatively seismically quiescent, several recent earthquakes are suspected to have been triggered by industrial activities (near Snyder/Cogdell, Karnes City/Fashing, the Dallas-Fort Worth metroplex, and Timpson). These earthquakes have nodal plane geometries consistent with the observed stress field, indicating that they are occurring on faults that are already likely to be active. At Timpson, aligned earthquake epicenters suggest slip along a NW striking and/or multiple NE striking planes [*Frohlich et al.*, 2014]. Our analysis indicates that the NE striking planes are compatible with slip in the observed stress state despite being closer to parallel with $S_{Hmax}$ than would be ideal for slip. In contrast, slip on the NW striking planes requires pore pressure perturbations in excess of the hydraulic fracturing pressure. Near the Dallas-Fort Worth metroplex, the stress regime transitions rapidly from strike-slip faulting north of Fort Worth to normal faulting to the south, implying that the orientations of faults most likely to produce earthquakes varies systematically across this area.

**Acknowledgments**
This research was funded by the Stanford Center for Induced and Triggered Seismicity (SCITS). The authors are grateful to Apache Corporation, ConocoPhillips, Devon Energy, Newfield Energy, and XTO Energy for contributing stress data and to O. Heidbach for sharing unpublished data from the 2016 release of the World Stress Map. The authors thank Cliff Frohlich and an anonymous reviewer for helpful and constructive comments that improved the manuscript. The new stress data and compiled $A_\varphi$ (faulting regime) values are available in the supporting information (Tables S1 and S2). The authors declare no financial conflicts of interest.

## References

Alt, R. C., II, and M. D. Zoback (2016), In-situ stress and active faulting in Oklahoma, *Bull. Seismol. Soc. Am.*, in press.
Crone, A. J., and K. V. Luza (1990), Style and timing of Holocene surface faulting on the Meers fault, southwestern Oklahoma, *Bull. Geol. Soc. Am.*, *102*(1), 1–17, doi:10.1130/0016-7606(1990)102<0001:SATOHS>2.3.CO;2.
Darold, A. P., and A. A. Holland (2015), Preliminary Oklahoma optimal fault orientations, *Oklahoma Geol. Surv. Open File Rep., OF4–2015*.
Davis, S. D., and W. D. Pennington (1989), Induced seismic deformation in the Cogdell oil field west Texas, *Bull. Seismol. Soc. Am.*, *79*(5), 1477–1494.
Doser, D. I., M. R. Baker, and D. B. Mason (1991), Seismicity in the War-Wink gas field, Delaware Basin, west Texas, and its relationship to petroleum production, *Bull. Seismol. Soc. Am.*, *81*(3), 971–986, doi:10.1016/0148-9062(92)93679-E.
Ewing, T. E., and Lopez, R. F., compilers (1991), Principal structural features, Gulf of Mexico Basin, in Salvador, A., ed., The Gulf of Mexico Basin: Boulder, Colo., Geol. Soc. of Am., Geology of North America, v. J, plate 2, scale 1:2,500,000.
Ewing, T. E., R. T. Budnik, J. T. Ames, D. M. Ridner, and R. L. Dillon (1990), Tectonic map of Texas: University of Texas at Austin, Bureau of Economic Geology, 4 sheets, scale 1:750,000.
Fan, Z., P. Eichhubl, and J. F. W. Gale (2016), Geomechanical analysis of fluid injection and seismic fault slip for the $M_w$ 4.8 Timpson, Texas, earthquake sequence, *J. Geophys. Res. Solid Earth*, *121*, 2798–2812, doi:10.1002/2016JB012821.
Frohlich, B. C., H. Deshon, B. Stump, C. Hayward, M. Hornbach, and J. I. Walter (2016), A historical review of induced earthquakes in Texas, *Seismol. Res. Lett.*, *87*(3), 1–59, doi:10.1785/0220160016.
Frohlich, C., and M. Brunt (2013), Two-year survey of earthquakes and injection/production wells in the Eagle Ford Shale, Texas, prior to the $M_w$4.8 20 October 2011 earthquake, *Earth Planet Sci. Lett.*, *379*, 56–63, doi:10.1016/j.epsl.2013.07.025.
Frohlich, C., C. Hayward, B. W. Stump, and E. Potter (2011), The Dallas-Fort Worth earthquake sequence: October 2008 through May 2009, *Bull. Seismol. Soc. Am.*, *101*(1), 327–340, doi:10.1785/0120100131.
Frohlich, C., W. L. Ellsworth, W. A. Brown, M. Brunt, J. H. Luetgert, T. MacDonald, and S. Walter (2014), The 17 May 2012 *M* 4.8 earthquake near Timpson, East Texas: An event possibly triggered by fluid injection, *J. Geophys. Res. Solid Earth*, *119*, 581–593, doi:10.1002/2013JB010755.
Gan, W., and C. Frohlich (2013), Gas injection may have triggered earthquakes in the Cogdell oil field, Texas, *Proc. Natl. Acad. Sci. U.S.A.*, *110*(47), 18,786–18,791, doi:10.1073/pnas.1311316110.
Green, G. N., and G. Jones (1997), The digital geologic map of New Mexico in ARC/INFO Format, *U.S. Geol. Surv. Open File Rep. Ser., 97–52*.
Heidbach, O., M. Tingay, A. Barth, J. Reinecker, D. Kurfeß, and B. Müller (2010), Global crustal stress pattern based on the World Stress Map database release 2008, *Tectonophysics*, *482*(1-4), 3–15, doi:10.1016/j.tecto.2009.07.023.
Herrmann, R. B. (2016), Timpson, Texas earthquakes of May, 2012 http://www.eas.slu.edu/eqc/eqc_mt/MECH.NA/20120517081201/TimpsonTX.pdf (accessed July 2016).
Herrmann, R. B., H. M. Benz, and C. J. Ammon (2011), Monitoring the earthquake source process in North America, *Bull. Seismol. Soc. Am.*, *101*(6), 2609–2625, doi:10.1785/0120110095.
Hornbach, M. J., et al. (2015), Causal factors for seismicity near Azle, Texas, *Nat. Commun.*, *6*(6728), 6728, doi:10.1038/ncomms7728.
Hornbach, M. J., M. Jones, M. Scales, H. R. DeShon, M. B. Magnani, C. Frohlich, B. Stump, C. Hayward, and M. Layton (2016), Ellenburger wastewater injection and seismicity in North Texas, *Phys. Earth Planet. In.*, doi:10.1016/j.pepi.2016.06.012.
Hurd, O., and M. D. Zoback (2012), Intraplate earthquakes, regional stress and fault mechanics in the central and eastern U.S. and Southeastern Canada, *Tectonophysics*, *581*, 182–192, doi:10.1016/j.tecto.2012.04.002.
Justinic, A. H., B. W. Stump, C. Hayward, and C. Frohlich (2013), Analysis of the Cleburne, Texas, earthquake sequence from June 2009 to June 2010, *Bull. Seismol. Soc. Am.*, *103*(6), 3083–3093, doi:10.1785/0120120336.

Madole, R. F. (1988), Stratigraphic evidence of Holocene faulting in the mid-continent: The Meers fault, southwestern Oklahoma, *Geol. Soc. Am. Bull.*, *100*(3), 392–401, doi:10.1130/0016-7606(1988)100<0392:SEOHFI>2.3.CO;2.

Perry, F. V., W. S. Baldridge, and D. J. DePaolo (1987), Role of asthenosphere and lithosphere in the genesis of late Cenozoic basaltic rocks from the Rio Grande Rift and adjacent regions of the southwestern United States, *J. Geophys. Res.*, *92*(B9), 9193–9213, doi:10.1029/JB092iB09p09193.

Ricketts, J. W., K. E. Karlstrom, A. Priewisch, L. J. Crossey, V. J. Polyak, and Y. Asmerom (2014), Quaternary extension in the Rio Grande Rift at elevated strain rates recorded in travertine deposits, central New Mexico, *Lithosphere*, *6*(1), 3–16, doi:10.1130/L278.1.

Seager, W. R., and P. Morgan (1979), Rio Grande Rift in southern New Mexico, west Texas, and northern Chihuahua: Rio Grande Rift, *Tectonics and magmatism*, *14*, 87–106, doi:10.1029/SP014p0087.

Simpson, R. W. (1997), Quantifying Anderson's fault types, *J. Geophys. Res.*, *102*(B8), 17,909–17,919, doi:10.1029/97JB01274.

Sone, H., and M. D. Zoback (2014), Viscous relaxation model for predicting least principal stress magnitudes in sedimentary rocks, *J. Petrol. Sci. Eng.*, *124*, 416–431, doi:10.1016/j.petrol.2014.09.022.

Vavryčuk, V. (2014), Iterative joint inversion for stress and fault orientations from focal mechanisms, *Geophys. J. Int.*, *199*(1), 69–77, doi:10.1093/gji/ggu224.

Vermylen, J., and M. D. Zoback (2011), Hydraulic fracturing, microseismic magnitudes, and stress evolution in the Barnett shale, Texas, USA in SPE Hydraulic Fracturing Technology Conference, Society of Petroleum Engineers, SPE 140507, 15 p., doi:10.2118/140507-MS.

Walsh, F. R., III, and M. D. Zoback (2016), Probabilistic assessment of potential fault slip related to injection-induced earthquakes: Application to north central Oklahoma, USA, *Geology*, doi:10.1130/G38275.1.

Walter, J. I., P. J. Dotray, C. Frohlich, and J. F. W. Gale (2016), Earthquakes in northwest Louisiana and the Texas–Louisiana border possibly induced by energy resource activities within the Haynesville Shale Play, *Seismol. Res. Lett.*, *87*(2A), 285–294, doi:10.1785/0220150193.

Zoback, M. D. (2010), *Reservoir Geomechanics*, Cambridge Univ. Press, New York.

Zoback, M. L. (1992), First- and second-order patterns of stress in the lithosphere: The World Stress Map Project, *J. Geophys. Res.*, *97*(B8), 11,703–11,728, doi:10.1029/92JB00132.

Zoback, M. L., and M. D. Zoback (1980), State of stress in the conterminous United States, *J. Geophys. Res.*, *85*(B11), 6113–6156, doi:10.1029/JB085iB11p06113.

Zoback, M. L., and M. D. Zoback (1989), Chapter 24: Tectonic stress field of the continental United States, *Geol. Soc. Am. Mem.*, *172*, 523–540.